

cy1

**COMBINED EFFECTS OF VISCOUS INTERACTION
AND IDEAL SOURCE FLOW ON PRESSURE AND HEAT-
TRANSFER DISTRIBUTIONS OVER HEMISPHERE
CYLINDERS AT $M_{\infty} \sim 18$**



R. H. Eaves, Jr. and Clark H. Lewis
ARO, Inc.

This document has been approved for public release
its distribution is unlimited. *Per DOE TR-75/5
AD A04700
Dtd July 1975*

July 1965

PROPERTY OF U. S. AIR FORCE
AEDC LIBRARY
AF 40(600)1200

**VON KÁRMÁN GAS DYNAMICS FACILITY
ARNOLD ENGINEERING DEVELOPMENT CENTER
AIR FORCE SYSTEMS COMMAND
ARNOLD AIR FORCE STATION, TENNESSEE**

AEDC TECHNICAL LIBRARY



5 0720 0003 1901 1E000 0270

NOTICES

When U. S. Government drawings specifications, or other data are used for any purpose other than a definitely related Government procurement operation, the Government thereby incurs no responsibility nor any obligation whatsoever, and the fact that the Government may have formulated, furnished, or in any way supplied the said drawings, specifications, or other data, is not to be regarded by implication or otherwise, or in any manner licensing the holder or any other person or corporation, or conveying any rights or permission to manufacture, use, or sell any patented invention that may in any way be related thereto.

Qualified users may obtain copies of this report from the Defense Documentation Center.

References to named commercial products in this report are not to be considered in any sense as an endorsement of the product by the United States Air Force or the Government.

COMBINED EFFECTS OF VISCOUS INTERACTION
AND IDEAL SOURCE FLOW ON PRESSURE AND HEAT-
TRANSFER DISTRIBUTIONS OVER HEMISPHERE
CYLINDERS AT $M_\infty = 18$

R. H. Eaves, Jr. and Clark H. Lewis
ARO, Inc.

This document has been approved for public release
and its distribution is unlimited. *Per DDC TR-75/5*
AD A011700
Dtd July, 1975

FOREWORD

The work reported herein was sponsored by Arnold Engineering Development Center (AEDC), Air Force Systems Command (AFSC), Arnold Air Force Station, Tennessee under Program Element 62405334, Project 8953, Task 895303.

The results of the research presented were obtained by ARO, Inc. (a subsidiary of Sverdrup and Parcel, Inc.), contract operator of the AEDC under Contract AF 40(600)-1200. Experimental data were obtained under ARO Project No. VT3503, the analysis was made under ARO Project No. VW3507, and the report was submitted by the authors on June 30, 1965.

The authors are pleased to acknowledge the assistance of various individuals. P. C. Shelton of the von Kármán Gas Dynamics Facility (VKF), Hypervelocity Branch, ARO, Inc., provided some unpublished experimental data at $M_\infty = 19$. E. G. Burgess III, W. J. Phares, and W. C. Moger of the Engineering Support Facility, Scientific Computing Branch, ARO, Inc., were responsible for developing the computing machine programs and providing the numerical solutions presented herein.

This technical report has been reviewed and is approved.

Larry R. Walter
1st Lt, USAF
Gas Dynamics Division
DCS/Research

Donald R. Eastman, Jr.
DCS/Research

ABSTRACT

The combined effects of ideal source flow and viscous interaction on the pressure and heat-transfer distributions over hemisphere-cylinders are presented, and a comparison is made with experimental data from two of the AEDC-VKF hotshot tunnels. Ideal gas characteristics solutions for the inviscid flow field over the hemisphere-cylinders were obtained for ideal source flow fields matched to the tunnel geometry. The inviscid and viscous (laminar boundary layer) flow fields were iterated, and the resulting pressure and heat-transfer distributions were compared with the experimental data. Ideal gas analyses made at $M_\infty = 18$ predicted pressure and heat-transfer distributions over a 4-in. -diam model in the 100-in. hotshot Tunnel F, and pressure distributions for a similar model in the 50-in. hotshot Tunnel H were found in reasonably good agreement with the experimental data.

CONTENTS

| | <u>Page</u> |
|---|-------------|
| ABSTRACT | iii |
| NOMENCLATURE | vi |
| I. INTRODUCTION | 1 |
| II. THEORETICAL CONSIDERATIONS. | 2 |
| III. APPARATUS | |
| 3.1 Wind Tunnels. | 5 |
| 3.2 Models, Instrumentation, and Precision. | 5 |
| IV. RESULTS AND DISCUSSION | |
| 4.1 Pressure Distributions | 7 |
| 4.2 Heat-Transfer Distributions | 8 |
| V. CONCLUDING REMARKS | 8 |
| REFERENCES | 9 |

ILLUSTRATIONS

Figure

| | |
|---|----|
| 1. Hemisphere-Cylinder in Ideal Source Flow | 11 |
| 2. AEDC-VKF Hotshot Tunnels | |
| a. Tunnel HS1. | 12 |
| b. Tunnel H. | 12 |
| c. Tunnel F. | 12 |
| 3. Inviscid Surface Pressure Distributions over a 4-in. -diam Hemisphere-Cylinder at $M_\infty = 18$ | 13 |
| 4. The Combined Effects of Viscous Interaction and Ideal Source Flow on the Pressure Distribution in Tunnel H | 14 |
| 5. The Effects of Iteration on the Displacement Thickness over a 4-in. -diam Hemisphere-Cylinder in Tunnel F | 15 |
| 6. Scale Effects on Surface Pressure Distribution in Ideal Source Flow in Tunnel F | 16 |
| 7. Comparison of Predicted and Experimental Pressure Distributions | |
| a. Tunnel F. | 17 |
| b. Tunnel H. | 18 |

| Figure | <u>Page</u> |
|---|-------------|
| 8. Comparison of Predicted and Experimental Heat-Transfer Distribution over a 4-in. -diam Model in Tunnel F | 19 |

TABLES

| | |
|--|----|
| I. Tunnel Conditions | 21 |
| II. Tunnel F 4-in. -diam Model Experimental Data | 22 |
| III. Tunnel H Experimental Data | 23 |

NOMENCLATURE

Unless otherwise noted, all lengths are nondimensionalized by the nose (sphere) radius

| | |
|-----------------|---|
| L | Length from tunnel nozzle apex to exit radius, in. |
| M | Mach number |
| p | Pressure, psia |
| p'_0 | Normal shock stagnation (pitot) pressure at M_∞ , psia |
| Pr | Prandtl number |
| \dot{q} | Heat-transfer rate, Btu/ft ² -sec |
| $\dot{q}(0)$ | Stagnation heat-transfer rate, Btu/ft ² -sec |
| R | Radius normal to axis of symmetry |
| R_{eff} | Effective wall radius, $R_w(x) + \delta^{*(n-1)} \cos \alpha$ |
| $Re_\infty/in.$ | Free-stream unit Reynolds number, $\rho_\infty u_\infty / \mu_\infty$ |
| R_N | Nose (sphere) radius |
| R_T | Tunnel nozzle exit radius, in. |
| T | Temperature, °K |
| TVC | Transverse curvature |
| u | Tangential velocity component, ft/sec |
| v | Normal velocity component, ft/sec |

| | |
|------------|---|
| x | Surface distance measured from the stagnation point |
| y | Distance normal to the surface |
| z | Axial distance measured from the stagnation point |
| α | Angle of tangent to the surface at x |
| γ | Ratio of specific heats |
| δ | Total boundary-layer thickness, $u/u_e = 0.995$ |
| δ^* | Boundary-layer displacement thickness |
| η | Transformed coordinate normal to the wall, $\sqrt{u_e/\rho^*\mu^*x} \int_0^y \rho dy$ |
| θ_T | Tunnel nozzle cone angle, deg |
| μ | Dynamic viscosity |
| ρ | Mass density |

SUBSCRIPTS

| | |
|----------|---|
| e | Local conditions at the edge of the boundary layer |
| $i. w.$ | Inviscid wall |
| o | Free-stream stagnation conditions |
| w | Surface (wall) conditions |
| ∞ | Free-stream conditions |
| $*$ | Reference conditions at the sonic point on the body |

SUPERSCRIPTS

| | |
|-------|---|
| (n) | Iteration index corresponding to the pressure distribution over the effective body $R_{\text{eff}}^{(n)}(x) = R_w(x) + \delta^{*(n-1)} \cos \alpha$ |
|-------|---|

SECTION I INTRODUCTION

Most hypersonic shock tunnels and hotshot-type tunnels in operation today use conical, axisymmetric nozzles. Some are equipped with contoured nozzles but almost certainly the original research done in those tunnels made use of simple conical nozzles. At $M_\infty \leq 10$ and/or high Reynolds numbers, the complications of viscous interaction and other second-order boundary-layer effects are usually small. However, at $M_\infty = 20$, the Reynolds numbers are usually sufficiently low such that second-order boundary-layer effects should be considered. The experimentalist's problem is further complicated when he tries to analyze the experimental data taken in a wind tunnel with a conical nozzle since the growth rate of the boundary layer on the nozzle wall is nonuniform. The actual (experimental) nozzle flow field deviates from an ideal source flow, and the origin of the experimental "source" flow must be determined from experimental measurements (usually pitot pressure surveys of the test section).

Much of the previous work in this area has been directed toward estimating the effects of ambient source flow effects on (inviscid) model pressures, forces, and moments. Whitfield and Norfleet (Ref. 1) applied Newtonian theory to correct the experimental pressure distribution data of Lewis (Ref. 2) taken in the AEDC-VKF 16-in. hotshot Tunnel HS1. For slender bodies with small nose bluntness, Whitfield and Norfleet found significant source flow effects on the model surface pressure and therefore on the inviscid pressure drag.

Burke and Bird (Ref. 3) considered the effects of source flow on the forces and moments of a delta wing in the Cornell Aeronautical Laboratory (CAL) reflected shock tunnel. They also applied the Newtonian theory to estimate the effects of source flow on the pressure distribution over the delta wing and found significant effects on the forces and moments, especially at high angles of attack, and on control surfaces.

Hall (Ref. 4) applied a small perturbation analysis to study the effects of source flow on sharp and blunt nosed, two-dimensional and axisymmetric slender bodies. The primary interest in that study was the effects of source flow on surface pressure distributions and shock shapes. Large effects of source flow on the pressure distributions were found especially on the sharp nosed bodies and, in the case of blunt nosed bodies, far downstream of the nose dominated region.

The present study is concerned with comparing the results of experimental measurements made in conical nozzles with theoretical predictions

of ideal source flow with the coupled effects of the viscous boundary layer on the external, inviscid flow field and hence on the wall pressure and heat-transfer distributions. The inviscid flow field is iterated with the viscous boundary-layer solution until there is negligible change in the "effective" body geometry and thus in the pressure distribution along the wall. The effective body is obtained by adding the displacement thickness to the geometric body. The resulting "effective" body is not consistent with physical requirements since the inviscid wall boundary condition ($v_{i,w} = 0$) is not satisfied along the displacement surface $\delta^*(x)$. The global continuity equation is, however, satisfied if the external flow field is irrotational. In the cases studied herein, the external inviscid flow field over the body is rotational, but the effects of shock generated external vorticity are not included.

In a recent paper, Lewis and Whitfield (Ref. 5) applied the methods used in the present analysis to estimate the effects of viscous interaction and transverse curvature on the pressure and heat-transfer distributions and the zero-lift drag of a spherically blunted cone at $M_\infty = 9$ and 18 in uniform parallel flow. The details which pertain to the present analysis will be given below. Both analyses used an ideal gas ($\gamma = 1.4$) characteristics solution and the compressible laminar boundary-layer theory of Clutter and Smith (Ref. 6). The heat-transfer distribution theory of Lees (Ref. 7) was also used in the present investigation for comparison with the theory of Clutter and Smith and the experimental results.

The purpose of the present report is to present comparisons of numerical predictions and experimental data taken in two hotshot-type wind tunnels of the AEDC-VKF: the 50- and the 100-in. hotshot tunnels (Gas Dynamic Wind Tunnels, Hypersonic (F) and (H)). The models considered were hemisphere-cylinders of 1 and 4 in. diameters and various lengths.

All inviscid flow field calculations in the present report were based on an ideal (point) source flow. It is shown below that ideal source flow substantially overestimates the Mach number gradient upon comparison with the limited experimental data available. However, since sufficient experimental data do not exist to adequately define an "effective" (experimental) origin and the flow angularity of the actual "source" flow, an ideal source flow model was used.

SECTION II THEORETICAL CONSIDERATIONS

The theoretical model used in the present study is shown in Fig. 1. The axis of symmetry of the hemisphere-cylinder model was coincident

with the hypersonic nozzle axis of symmetry, and the origin of the ideal source flow was the apex of the divergent nozzle. The subsonic portion of the blunt body flow was obtained from a uniform parallel flow inverse solution at $M_\infty = 18$. The intersection of the initial line and the shock wave was located in the exit plane of the nozzle. The nozzle half-angle θ_T , exit radius R_T , and length L of the three hotshot tunnel nozzles are shown on Fig. 1. The horizontal component of the free-stream Mach number at the intersection of the velocity vector from the origin of the ideal source flow to the intersection of the initial line and shock wave was taken to be 18, and the pressure at this point was assumed to be 1 atm. For calculation purposes all lengths were nondimensionalized with respect to the nose (sphere) radius of the model.

The supersonic inviscid flow field over the body was obtained from an ideal gas ($\gamma = 1.4$) characteristic solution. The initial supersonic data were obtained from the uniform parallel flow inverse blunt body solution at $M_\infty = 18$. The boundary conditions along the wall (viz, $v_{1,w} = 0$) were unchanged from the usual parallel flow characteristic solution. The boundary conditions along the shock wave, however, were changed such that the origin of the velocity vector or ideal source flow coincided with the virtual apex of the divergent conical nozzle rather than at $-\infty$ as in the usual parallel flow case. The results then differ from the uniform parallel flow characteristic solution only in the change of the boundary conditions at the shock wave. It was assumed that the effects of source flow on the subsonic and transonic blunt body solution were negligible.

With the conditions along the wall determined from the characteristic solution, it was then possible to do a boundary-layer solution. The recent theory of Clutter and Smith (Ref. 6) was used in the present investigation. They transform the boundary-layer partial differential equations in the (x, y) plane to the (x, η) plane under the transformations

$$x = x \quad \text{and} \quad \eta = \sqrt{\frac{u_e}{\rho^* \mu^* x}} \int_0^y \rho dy$$

and solve the resulting momentum and energy equations by iteration retaining the nonsimilar and approximate transverse curvature terms.

For the calculations presented herein an ideal gas, a Prandtl number $Pr = Pr_w = 0.71$ (constant), and Sutherland's viscosity law were assumed. All calculations were made at $M_\infty = 18$ as described above and with wall-to-stagnation temperature ratio $T_w/T_0 = 0.066$. The ideal gas boundary-layer assumption is consistent with the inviscid flow field calculation, and comparison of equilibrium and ideal gas solutions for one-dimensional flow along the inviscid wall from stagnation conditions similar

to those in the wind tunnel have shown small differences despite the fact that the stagnation temperatures are relatively high. The variation of Prandtl number within the boundary layer was not known and the assumption of constant Prandtl number seemed reasonable. Similarly, for the range of temperatures and pressures in the present study, Sutherland's viscosity law for the gas (nitrogen) viscosity is a good one. The results of the first calculation denoted herein as the zeroth iteration yield a displacement thickness distribution $\delta^{*(0)}(x)$. The effective wall was determined in the usual way by adding the displacement thickness to the geometric wall, $R_{\text{eff}}(x) = R_w(x) + \delta^* \cos \alpha$.

For the highly cooled wall conditions considered here, the displacement thickness was negative over most of the spherical nose. To obtain the first iterated inviscid flow field solution, an approximation was made as illustrated on Fig. 1. The curve $S(z)$ was drawn tangent to the unit sphere at I and tangent to the effective wall as defined above at B, and $d^2S/dz^2 < 0$ was required between I and B. With this new approximate effective wall and the original initial supersonic data, the first iterated flow field solution was obtained. It was then possible to obtain the second boundary-layer solution (denoted herein as the first iteration) and thus a new $\delta^*(x)$ distribution. The effective wall in the supersonic region was obtained as before and similarly the next inviscid supersonic solution. This procedure can be continued in principle until there is negligible change in either $\delta^*(x)$ or $p_{\text{eff}}(x) = p_w(x)$. Fortunately, for the range of conditions considered herein only two iterations or three boundary-layer calculations were required.

The present analysis makes use of numerically "exact" solutions (viz., an inviscid ideal source flow field characteristic solution and non-similar laminar boundary-layer solution) and is approximate in the method of joining the inviscid-viscous solutions. Of primary interest in the present study is the displacement effect on the pressure and heat-transfer distributions along the surface. However, a few calculations were made to determine the effects of transverse curvature on the heat-transfer distribution. As Lewis and Whitfield (Ref. 5) found earlier in the case of spherically blunted cones, the effects of transverse curvature on the displacement thickness were negligible. Other second-order effects, especially shock generated external vorticity, should be included or at least approximately considered. However, at the present time, there are difficult problems to be solved regarding the boundary conditions at the outer edge of the boundary layer in the presence of both viscous and vorticity interactions. Crude estimates show that the effects of other second-order terms (namely, longitudinal curvature, slip, and temperature jump) should be negligible for the conditions presented herein provided the boundary-layer assumption remains valid.

SECTION III APPARATUS

3.1 WIND TUNNELS

The experimental data reported herein were obtained from the hotshot Tunnels H and F. For comparison purposes calculations are presented for the original hotshot Tunnel HS1. The hotshots are electric arc heated tunnels using nitrogen as a test gas. The gas is heated at constant volume and expanded through an axisymmetric convergent-divergent conical nozzle to the test section. These tunnels are illustrated in Fig. 2, and additional information can be found in Ref. 8. Tunnel operating conditions for the experimental data are shown in Table I, and the pressure and heat-transfer experimental data are given in Tables II and III.

3.2 MODELS, INSTRUMENTATION, AND PRECISION

Data are presented for two hemisphere-cylinder models, one 4 in. in diameter and the other 1 in. in diameter. Both models were made of aluminum in order to reduce their mass and thus minimize the sting oscillations.

The model wall temperature was essentially constant for the short duration of the test (approximately 50 msec) and was assumed to be 300°K. Therefore, the ratio of wall-to-stagnation temperature, T_w/T_o , varied essentially between 0.075 and 0.13 simulating the "cold wall" condition of practical interest in the hypersonic regime.

Test-section pitot pressures, model wall, and base pressures were measured with rapid response, variable reluctance pressure transducers which are described in detail in Ref. 9. Tunnel reservoir pressures were measured with strain gage-type transducers. The stagnation heat-transfer data on the hemisphere-cylinder probe used for monitoring the test-section conditions were measured with calorimeter-type transducers which use thermocouples as temperature sensors. These transducers are described in detail in Ref. 10.

The test-section heat-transfer rate on the hemisphere-cylinders and the pitot pressures were used in conjunction with the Fay-Riddell stagnation heat-transfer theory (Ref. 11) to determine the reservoir enthalpy. These data and the measured reservoir pressure were used to calculate the remaining flow conditions as described in Ref. 12. A discussion of the method of calculating reservoir conditions is given in Ref. 13.

The accuracy of the results from any high temperature test facility is, of course, a function not only of the uncertainty of the direct measurements but also of the validity of the assumptions used to obtain the test-section flow parameters. A repeatability of ± 10 percent in the stagnation heat-transfer rate measured on the monitoring probes in the test section along with other random errors led to the following estimated uncertainty for the experimental data presented.

| <u>Data</u> | <u>Uncertainty, percent</u> |
|--------------------|---------------------------------|
| Pressure | ± 5 |
| Heat-transfer rate | ± 10 |
| M_{∞} | ± 2 |
| $Re_{\infty}/in.$ | ± 15 |

SECTION IV RESULTS AND DISCUSSION

Before presenting the results of comparison of experiment and prediction for the pressure and heat-transfer distributions, a comparison of ideal source flow and experimental axial Mach number gradient for the hotshot tunnels is given below.

AXIAL MACH NUMBER GRADIENT PER FOOT

| | <u>Ideal Source Flow</u> | <u>Experimental</u> | <u>Source</u> |
|------------|--------------------------|---------------------|------------------------------------|
| Tunnel F | 0.114 | 0.064 | Ball (Ref. 14) |
| Tunnel H | 0.308 | 0.240 | Whitfield and Norfleet (Ref. 1) |
| Tunnel HS1 | 0.962 | 0.8 | Unpublished Data |

The experimental data for Tunnels F and HS1 were obtained from axial pitot pressure surveys, whereas the experimental value for the Tunnel H was obtained from a source flow correction of experimental data as obtained by Whitfield and Norfleet (Ref. 1). The ideal source flow is seen to substantially overpredict the gradient as might be expected since the nozzle wall boundary layer longitudinally turns the inviscid core flow and thus reduces the source flow effect. The ideal source flow gradient is in agreement with the formula given by Hall (Ref. 4) for the same effect.

The effects of ideal source flow on the pressure distribution over the 4-in. -diam hemisphere-cylinder in the three hotshot tunnels are shown

in Fig. 3. For comparison, a uniform parallel flow solution at $M_\infty = 18$ is also shown. As expected, the source flow effects are large in Tunnel HS1 (about 20 percent). As the tunnel size increases, the effects decrease until in Tunnel F the effects are very small (about 2 percent). As mentioned previously, all calculations were based on the model being on the tunnel centerline. However, if the model were placed off the tunnel axis the source flow effects would be significant even in Tunnel F.

The effects of viscous interaction and ideal source flow in Tunnel H are shown on Fig. 4 where again for comparison the uniform parallel flow solution is also shown. It is interesting to note that for this particular calculation the reduction in the pressure distribution due to source flow is almost equal to the viscous induced pressure increment.

The effects of iteration on the boundary-layer and inviscid flow field solutions are shown on Fig. 5. The calculation shown here, which is typical of the calculations presented, shows small differences between the first and second iteration. It should be noted that the zeroth and first iterations bound the variation of the displacement thickness since the pressure or Reynolds number is minimum and maximum, respectively, for those two iterations.

4.1 PRESSURE DISTRIBUTIONS

Figure 6 shows the results for the ideal source flow calculations for a 1-in. and 4-in. -diam model in Tunnel F. As might be expected, the scale difference for the two models has small effect on the ideal source flow pressure distribution. However, when the ideal source flow solution is combined with the viscous interaction calculation, there are significant differences. Figure 7a shows the ideal source flow calculation zeroth iteration for the 4-in. -diam model in Tunnel F. Also shown is the viscous induced pressure increment for the 1-in. and 4-in.-diam models where the increment for the 1-in. -diam model is roughly twice that of the 4-in. model. Experimental data taken on a 4-in. -diam model in Tunnel F are also shown. The numerical solution underestimates the mean of the experimental pressure distribution over the cylinder by approximately 5 percent. As previously mentioned, the ideal source flow gradient is approximately twice the experimental gradient in Tunnel F. Therefore, the numerical solution based on the experimental "source flow" would lie between curves based on parallel and ideal source flow. Although this only represents about a 2 percent increase in the prediction in Fig. 7a, it would improve the comparison with the experimental data.

Similar results are shown for Tunnel H in Fig. 7b. The trends in the numerical solutions and the viscous induced pressure increment are similar to those in Tunnel F. Again, comparisons are made with available experimental data for the 4-in. model and also two data points for a 1-in. -diam hemisphere-cylinder. It is evident that, compared with the inviscid, source flow solution, apparent viscous effects on the 1-in. -diam model are large, amounting to over 35 percent at $x \approx 2.17$. When viscous effects are taken into account, the discrepancy is reduced to 7 percent. Although viscous effects are much smaller in the case of the 4-in. -diam model, again a much better agreement is obtained with the boundary-layer iterated solutions.

4.2 HEAT-TRANSFER DISTRIBUTIONS

Heat-transfer calculations were made based on the combined ideal source flow and viscous interaction pressure distribution results. The results of those calculations are compared with experimental data taken in Tunnel F, and the results are shown on Fig. 8. The numerical results based on Lees' theory (Ref. 7) and the second iteration pressure distribution and experimentally measured pressure distribution are shown compared with the Clutter and Smith calculation with and without transverse curvature (TVC). Lees' theory based on the combined source flow and viscous interaction pressure distribution and also on the experimental pressure distribution is seen to be in good agreement with the experimental data. The Clutter and Smith calculations, both with and without transverse curvature, also overestimate the experimental data. The effects of transverse curvature on the heat-transfer distribution over the cylinder are approximately 12 percent, whereas the effects of transverse curvature on the displacement thickness (and thus pressure distribution) were found to be negligible.

SECTION V CONCLUDING REMARKS

The ideal gas ($\gamma = 1.4$) viscous boundary-layer theory of Clutter and Smith was iterated with an ideal source flow characteristic solution corresponding to the geometry of two hotshot tunnels, and comparisons were made with experimental data taken in those tunnels. The following results were obtained:

1. The present analysis of the combined effects of ideal source flow and viscous interaction underestimated the mean of the experimental pressure distribution on a 4-in. -diam model in the Tunnel F by approximately 5 percent. The prediction also overestimated the mean of the experimental heat-transfer distribution

data by approximately 3 percent. The trends were, however, well predicted, and the differences were approximately constant over the cylindrical portion of the model.

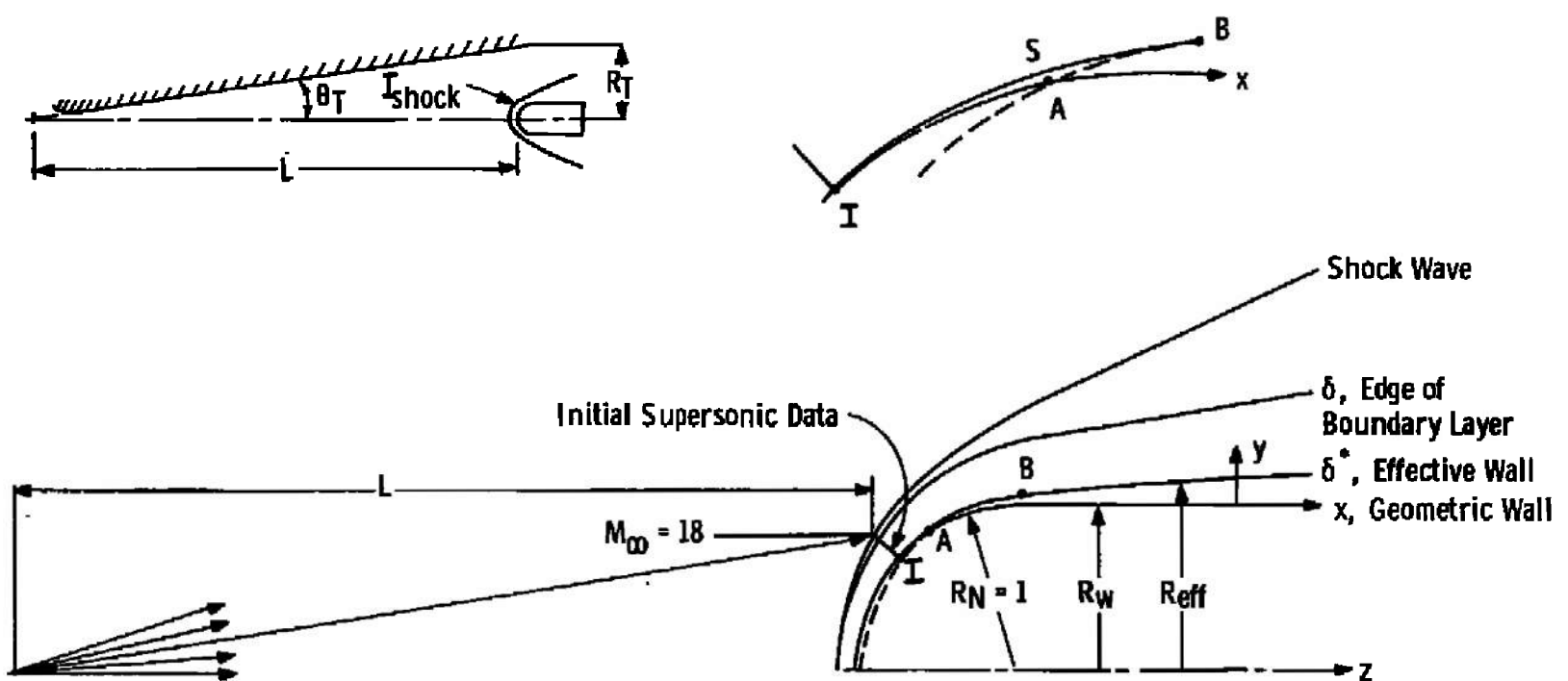
2. Similar calculations and comparisons of the pressure distribution in Tunnel H on the same 4-in. -diam model indicate reasonable agreement between the predicted and experimental pressure distribution.
3. Tunnel H results presented here indicate strong effects of source flow with compensatingly strong effects of viscous induced pressure. In some cases the results of the source flow and viscous interaction were seen to tend to cancel each other and thus predict a combined effect which was in reasonably good agreement with (inviscid) uniform parallel flow.

These results indicate that the experimentalist should exert caution when performing experiments in conical hypersonic nozzles, particularly when the nozzle half-angles are large and the Mach numbers are high. In any event, account of the combined effects of source flow and viscous interaction should be taken although in the present study both effects are only approximately treated. Also, other second-order effects including transverse curvature and vorticity interaction as they affect the pressure and heat-transfer distributions over slender blunted bodies should be considered further.

REFERENCES

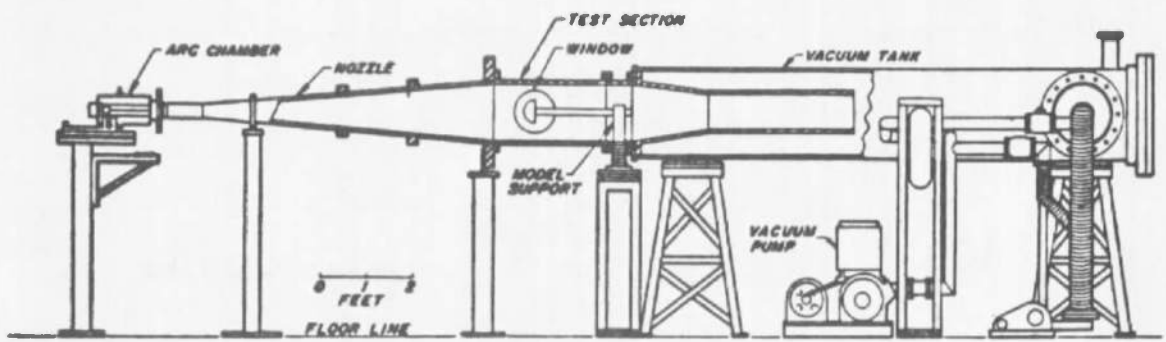
1. Whitfield, Jack D. and Norfleet, Glenn D. "Source Flow Effects in Conical Hypervelocity Nozzles." AEDC-TDR-62-116 (AD276724), June 1962.
2. Lewis, C. H. "Pressure Distribution and Shock Shape over Blunted Slender Cones at Mach Numbers 16 to 19." AEDC-TN-61-81 (AD261846), August 1961.
3. Burke, A. F. and Bird, K. D. "The Use of Conical and Contoured Expansion Nozzles in Hypervelocity Facilities." CAL Report No. 112, revised July 1962.
4. Hall, J. Gordon. "Effects of Ambient Nonuniformities in Flow over Hypersonic Test Bodies." CAL Report No. 128, August 1963.
5. Lewis, Clark H. and Whitfield, Jack D. "Theoretical and Experimental Studies of Hypersonic Viscous Effects." Paper presented at AGARD Specialists' Meeting on "Recent Developments in Boundary Layer Research", Naples, Italy, May 1965, Vol. III, AGARDograph 97.

6. Clutter, D. W. and Smith, A. M. O. "Solution of the General Boundary Layer Equations for Compressible Laminar Flow, Including Transverse Curvature." Douglas Aircraft Company Report LB 31088, February 1963, revised October 1964.
7. Lees, Lester. "Laminar Heat Transfer over Blunt-Nosed Bodies at Hypersonic Flight Speeds." Jet Propulsion, Vol. 26, No. 4, April 1956, p. 259.
8. Test Facilities Handbook, (5th Edition). "von Kármán Gas Dynamics Facility, Vol. 4." Arnold Engineering Development Center, July 1963.
9. Smotherman, W. E. "A Miniature Wafer-Style Pressure Transducer." AEDC-TR-60-11 (AD243875), October 1960.
10. Ledford, R. L. "A Device for Measuring Heat Transfer Rates in Arc-Discharge Hypervelocity Wind Tunnels." AEDC-TDR-62-64 (AD275740), May 1962.
11. Fay, J. A. and Riddell, F. R. "Theory of Stagnation Point Heat Transfer in Dissociated Air." Journal of the Aeronautical Sciences, Vol. 25, No. 2, February 1958.
12. Grabau, Martin; Smithson, H. K., Jr. and Little, W. J. "A Data Reduction Program for Hotshot Tunnels Based on the Fay-Riddell Heat-Transfer Rate Using Nitrogen at Stagnation Temperatures from 1500 to 5000°K." AEDC-TDR-64-50 (AD601070), June 1964.
13. Griffith, B. J. and Lewis, C. H. "A Study of Laminar Heat Transfer to Spherically Blunted Cones and Hemisphere-Cylinders at Hypersonic Conditions." AEDC-TDR-63-102 (AD408568), June 1963; also see AIAA Journal, Vol. 3, No. 3, March 1964, pp. 438-444.
14. Ball, Henry W. "Calibration of the 100-inch Hypervelocity Tunnel (F)." AEDC-TDR-63-46 (AD298279), March 1963.

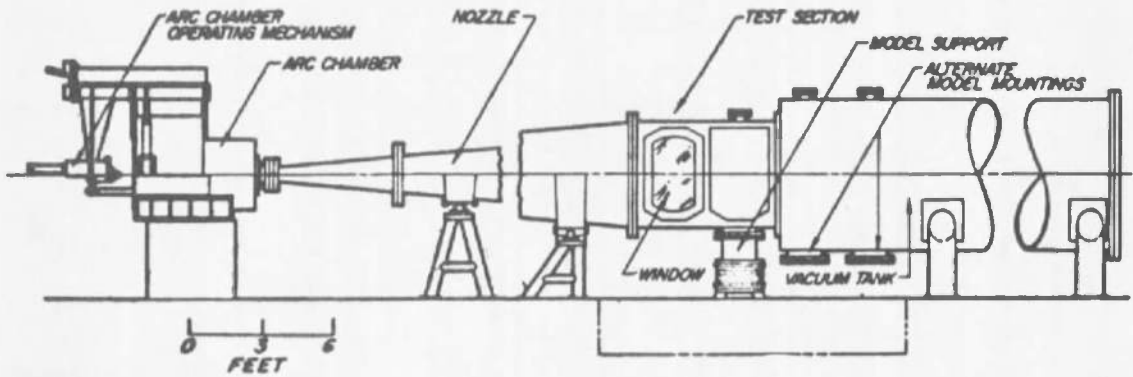


| | θ_T , deg | R_T , in. | L , in. |
|------------|------------------|-------------|-----------|
| Tunnel F | 4 | 54 | 772.0 |
| Tunnel H | 5 | 25 | 286.0 |
| Tunnel HS1 | 5 | 8 | 91.5 |

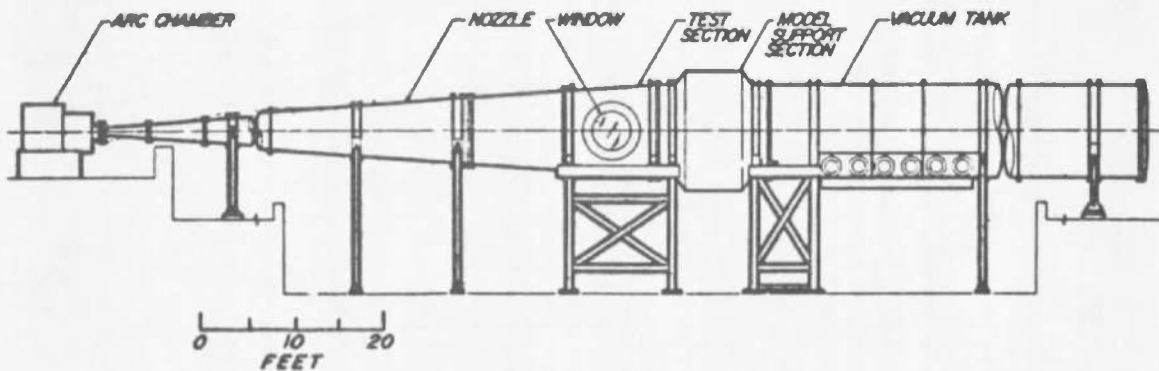
Fig. 1 Hemisphere-Cylinder in Ideal Source Flow



a. Tunnel HS1



b. Tunnel H



c. Tunnel F

Fig. 2 AEDC-VKF Hotshot Tunnels

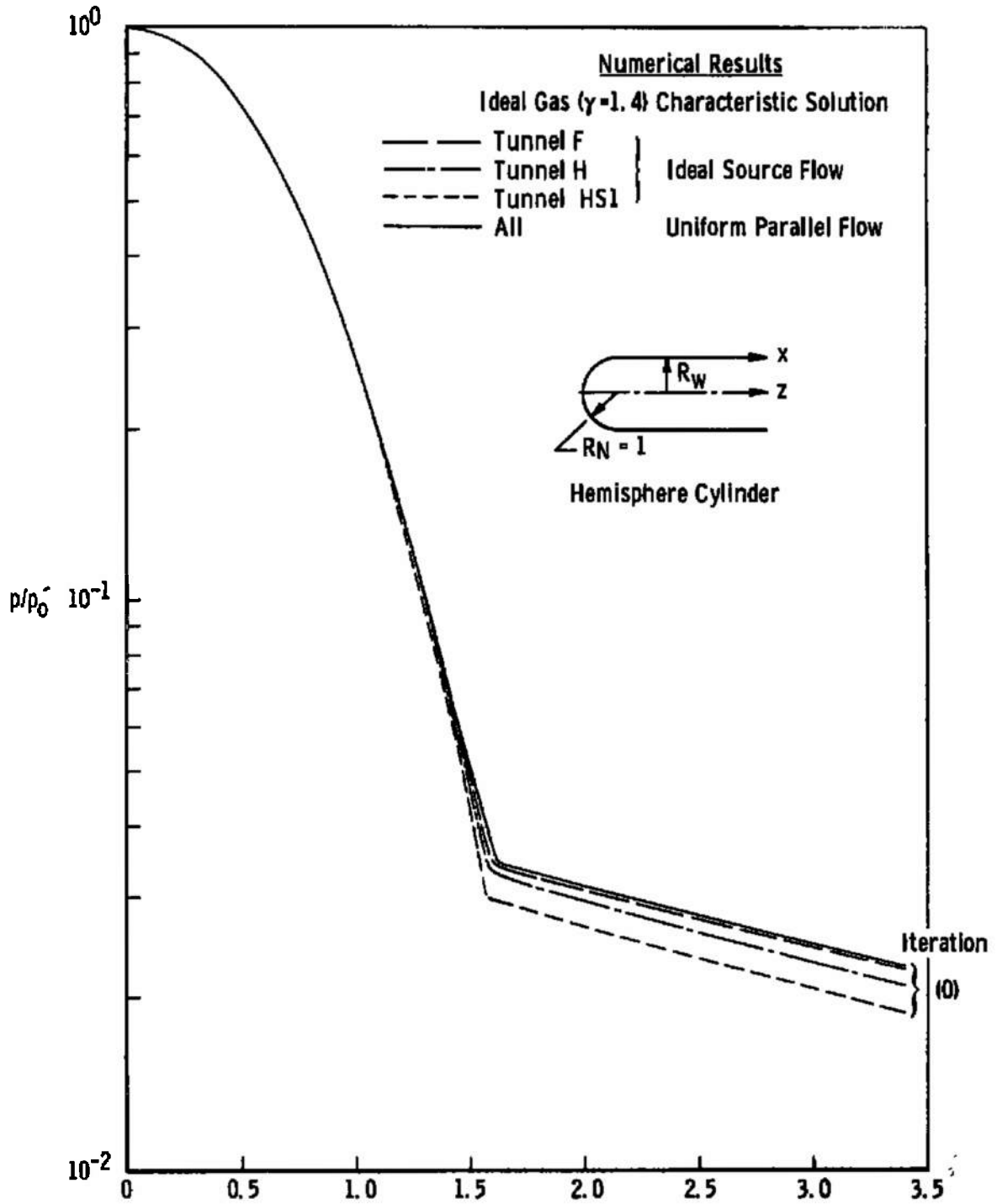


Fig. 3 Inviscid Surface Pressure Distributions over a 4-in.-diam Hemisphere-Cylinder at $M_\infty = 18$

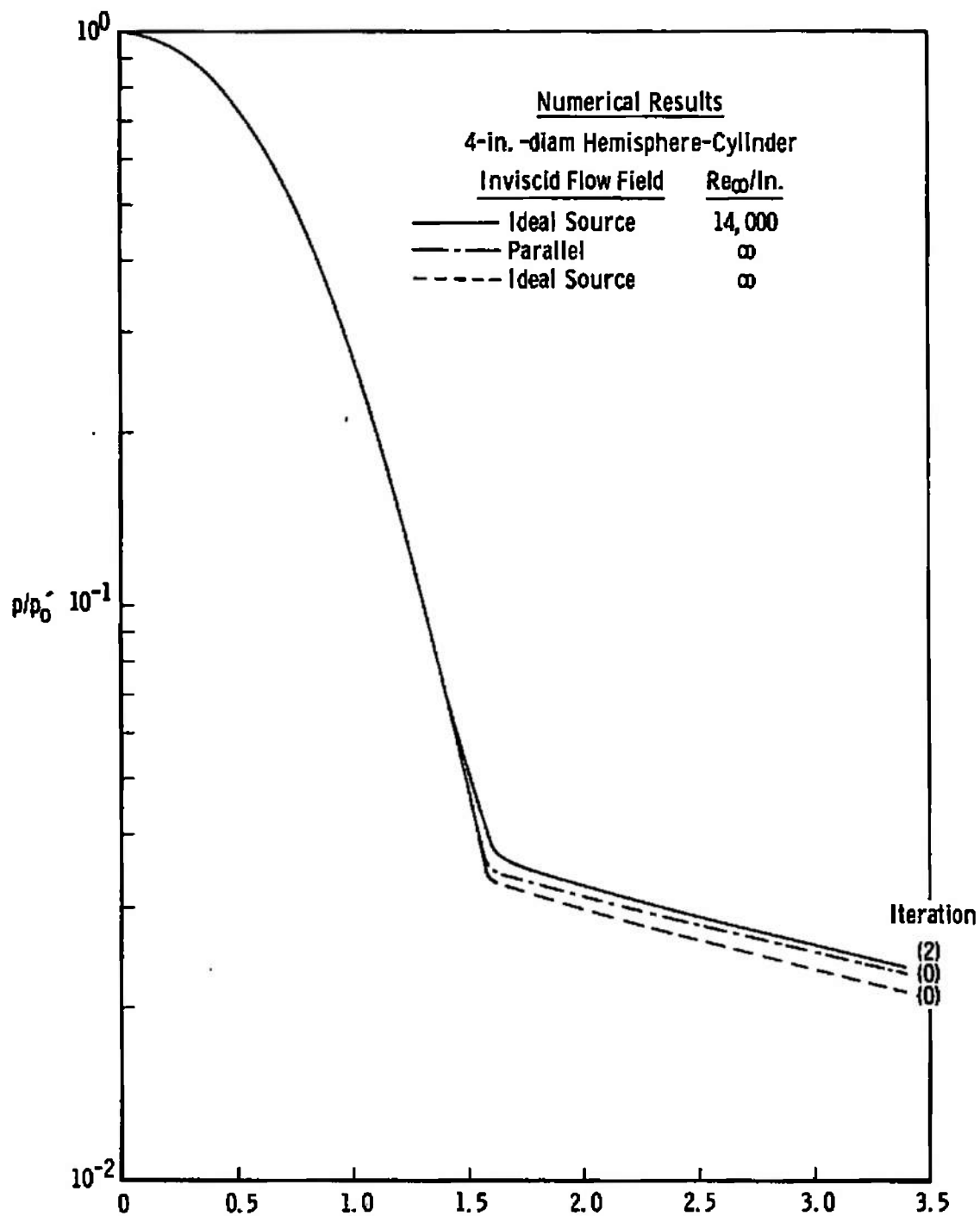


Fig. 4 The Combined Effects of Viscous Interaction and Ideal Source Flow on the Pressure Distribution in Tunnel H

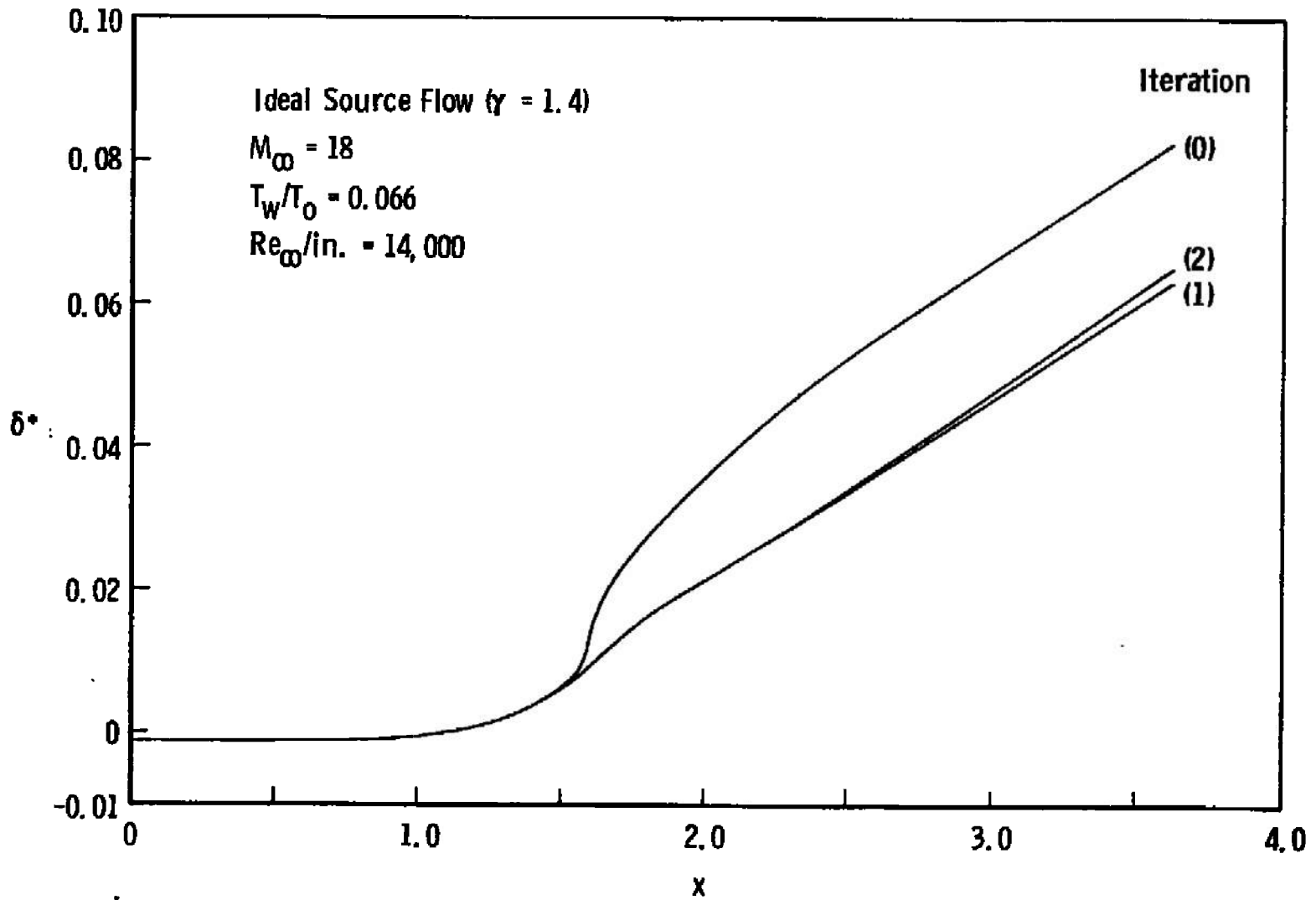


Fig. 5 The Effects of Iteration on the Displacement Thickness over a 4-in.-diam Hemisphere-Cylinder in Tunnel F

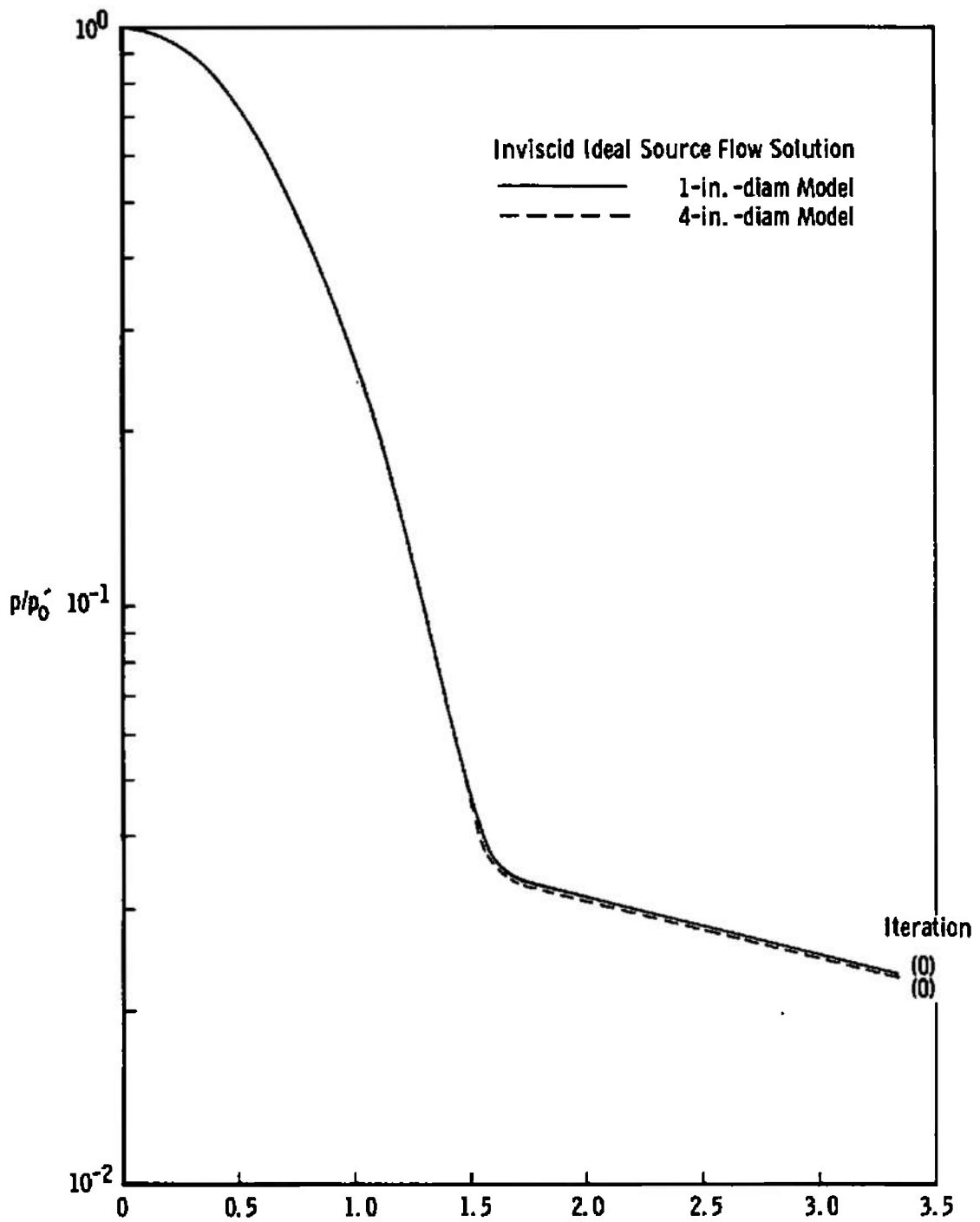


Fig. 6 Scale Effects on Surface Pressure Distribution
in Ideal Source Flow in Tunnel F

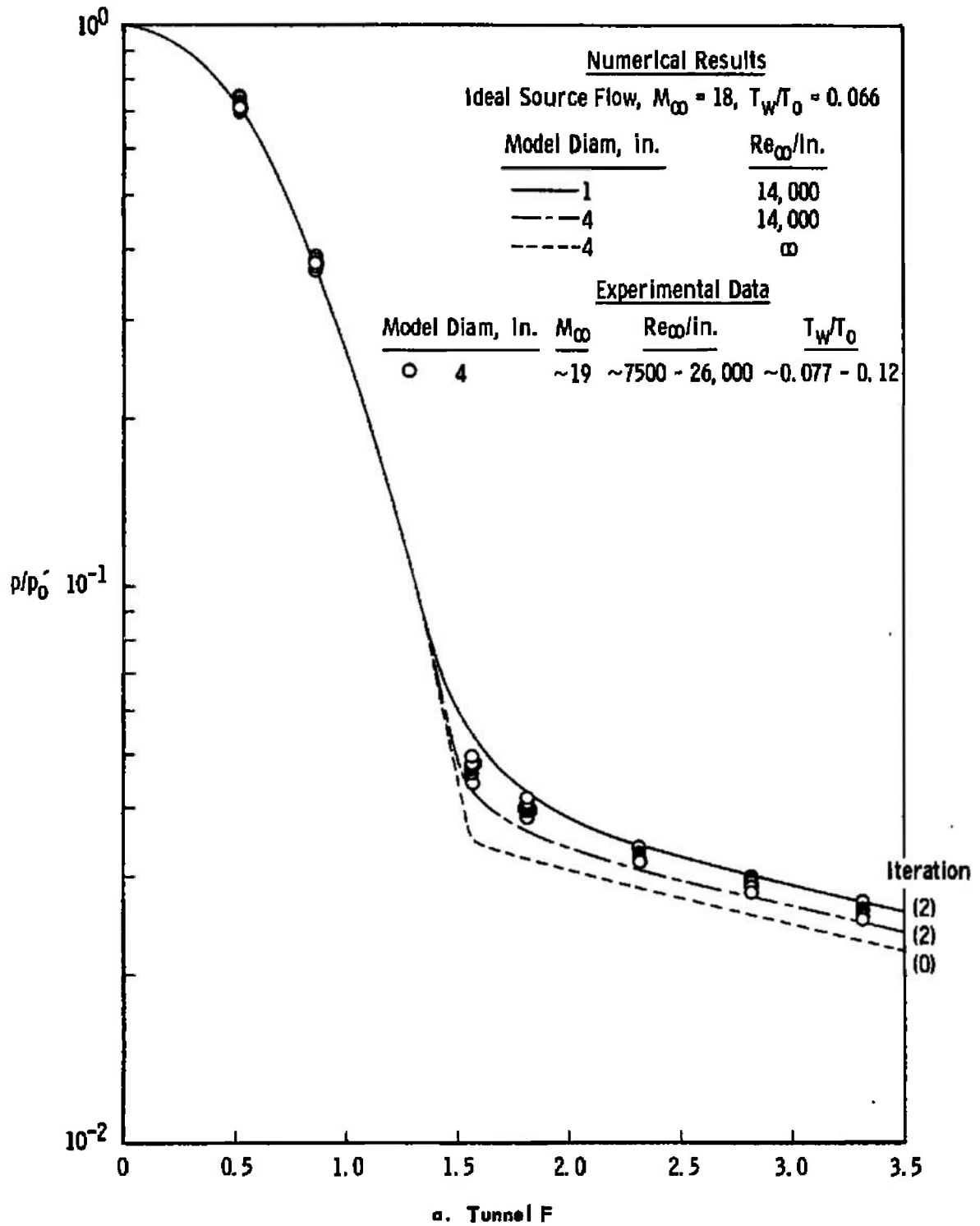
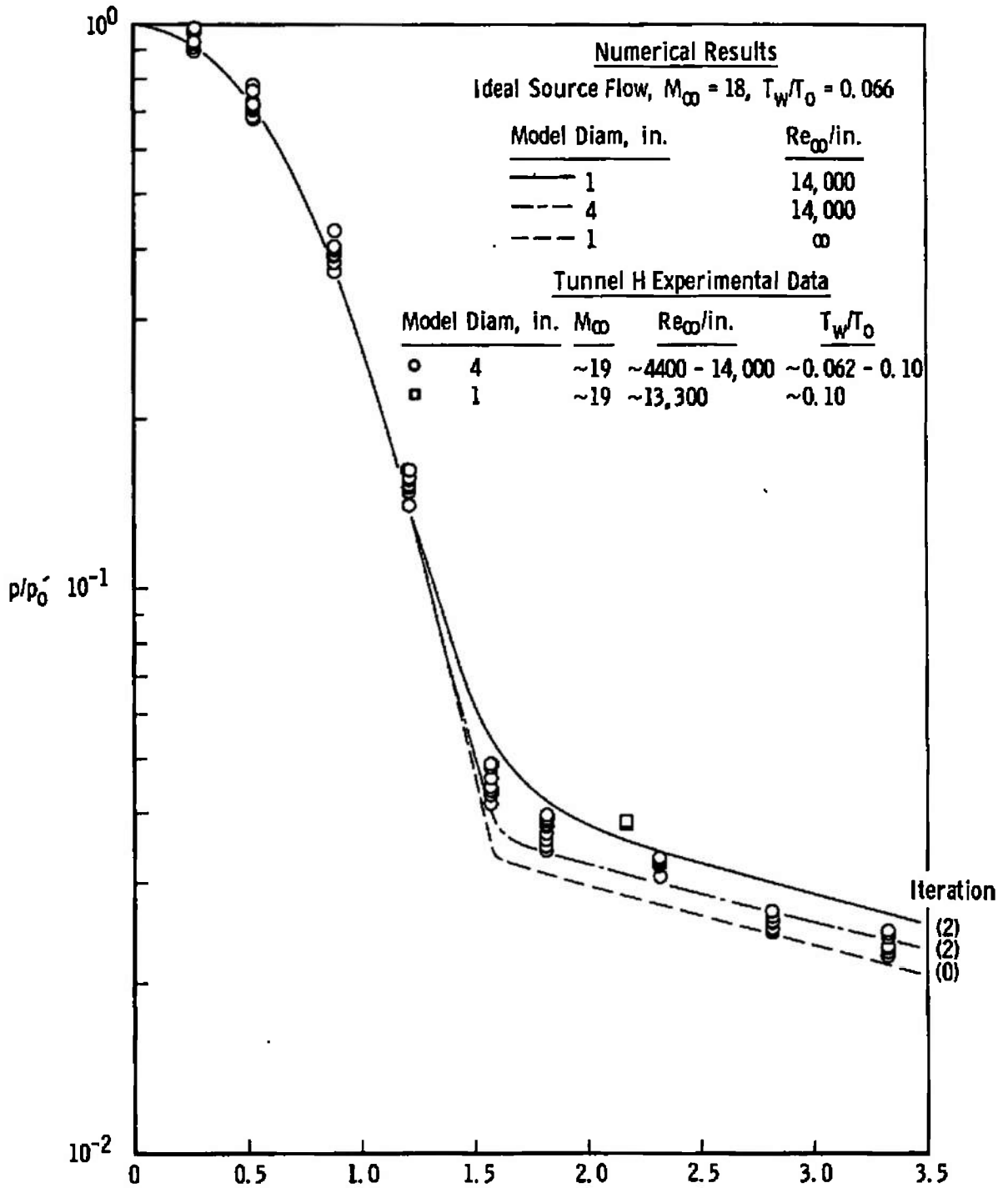


Fig. 7 Comparison of Predicted and Experimental Pressure Distributions



b. Tunnel H

Fig. 7 Concluded

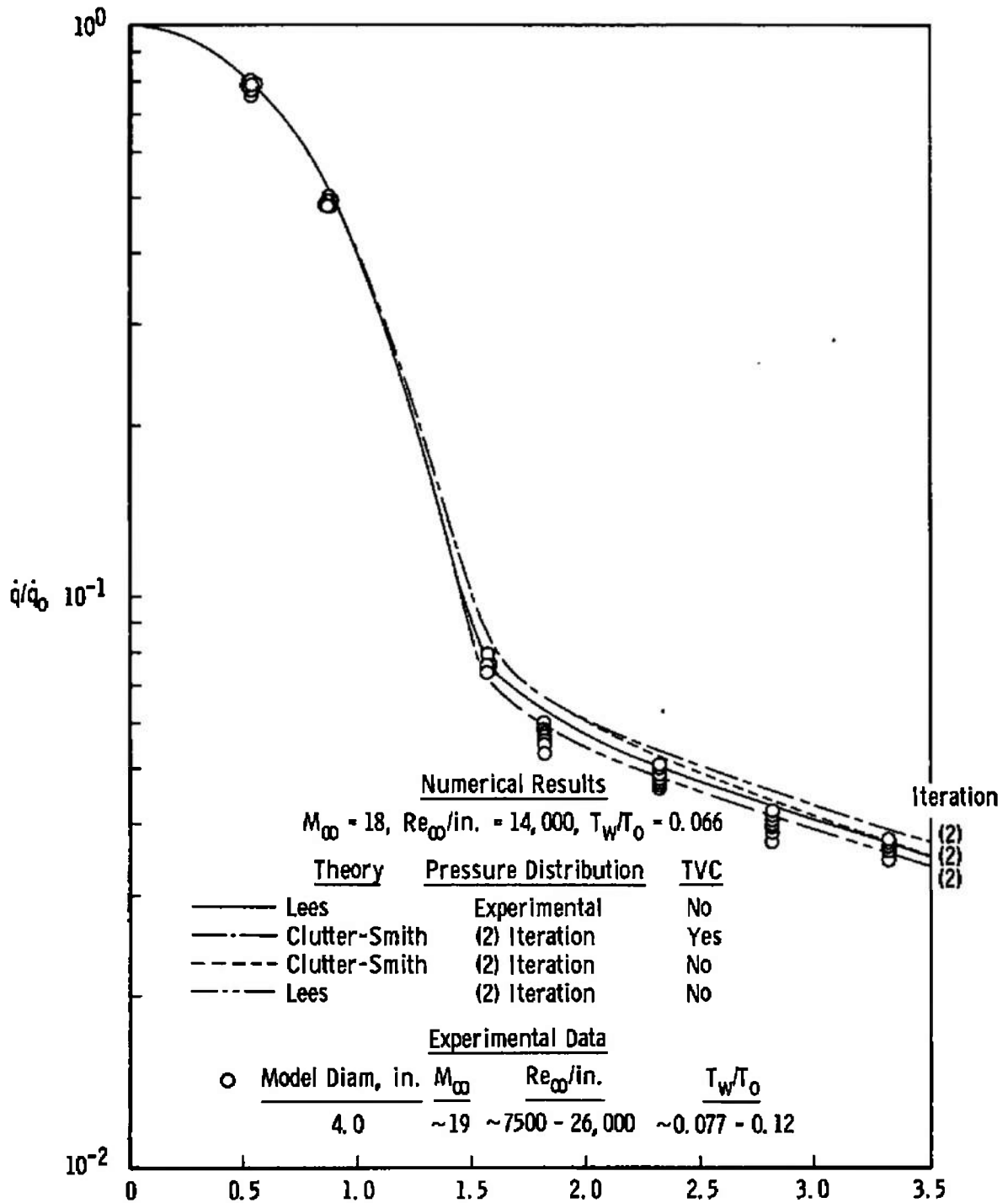


Fig. 8 Comparison of Predicted and Experimental Heat-Transfer Distribution over a 4-in.-diam Model in Tunnel F

TABLE I
TUNNEL CONDITIONS

a. Tunnel F

| Run | P_o | T_o | P_∞ | u_∞ | M_∞ | $Re_\infty/\text{in.}$ |
|-----|-------|-------|------------|------------|------------|------------------------|
| 723 | 7210 | 3440 | 0.00101 | 9,490 | 19.8 | 9,520 |
| 724 | 6810 | 3920 | 0.00116 | 10,170 | 19.0 | 7,480 |
| 725 | 7000 | 3730 | 0.00108 | 9,900 | 19.3 | 8,200 |
| 726 | 7360 | 2980 | 0.00105 | 8,790 | 20.1 | 13,120 |
| 727 | 7080 | 3750 | 0.00112 | 9,930 | 19.3 | 8,300 |
| 728 | 8170 | 2780 | 0.00250 | 8,470 | 18.1 | 23,170 |
| 729 | 8140 | 2630 | 0.00250 | 8,220 | 18.2 | 25,830 |

b. Tunnel H

| Run | P_o | T_o | P_∞ | u_∞ | M_∞ | $Re_\infty/\text{in.}$ |
|------|-------|-------|------------|------------|------------|------------------------|
| 1431 | 6950 | 3040 | 0.00140 | 8,900 | 19.0 | 13,500 |
| 1432 | 6720 | 3570 | 0.00130 | 9,700 | 18.8 | 13,000 |
| 1456 | 7100 | 3960 | 0.00159 | 10,300 | 18.2 | 8,450 |
| 1457 | 6080 | 4600 | 0.00050 | 11,100 | 20.8 | 3,550 |
| 1458 | 7080 | 4740 | 0.00057 | 11,300 | 20.8 | 4,370 |
| 1459 | 8010 | 3700 | 0.00150 | 9,930 | 18.8 | 9,930 |
| 1460 | 8250 | 4880 | 0.00175 | 11,500 | 18.0 | 6,300 |
| 1461 | 6760 | 3970 | 0.00055 | 10,200 | 20.8 | 5,410 |
| 1462 | 7550 | 3630 | 0.00161 | 9,780 | 18.5 | 9,900 |
| 1463 | 8560 | 3660 | 0.00181 | 9,820 | 18.5 | 11,600 |
| 1464 | 7390 | 3070 | 0.00142 | 8,940 | 19.1 | 13,800 |
| 1465 | 6460 | 3440 | 0.00152 | 9,500 | 18.3 | 10,400 |

TABLE II
TUNNEL F 4-IN.-DIAM MODEL EXPERIMENTAL DATA

a. Pressure Data, P/P_o'

| x Run | 0.524 | 0.873 | 1.57 | 1.82 | 2.32 | 2.82 | 3.32 | P_o' |
|------------|-------|-------|--------|--------|--------|--------|--------|--------|
| 723 | 0.714 | 0.378 | 0.0478 | 0.0400 | 0.0329 | 0.0294 | 0.0253 | 0.540 |
| 724 | 0.719 | 0.383 | 0.0481 | 0.0400 | 0.0325 | 0.0288 | 0.0264 | 0.534 |
| 725 | 0.746 | 0.393 | 0.0496 | 0.0415 | 0.0342 | 0.0301 | 0.0273 | 0.525 |
| 726 | 0.711 | 0.379 | 0.0468 | 0.0394 | 0.0320 | 0.0281 | 0.0251 | 0.609 |
| 727 | 0.706 | 0.368 | 0.0466 | 0.0396 | | 0.0298 | 0.0260 | 0.563 |
| 728 | 0.715 | | 0.0443 | 0.0382 | | 0.0289 | 0.0257 | 1.12 |
| 729 | 0.748 | | 0.0462 | 0.0394 | 0.0322 | 0.0294 | 0.0262 | 1.04 |

b. Heat-Transfer Data, \dot{q}/\dot{q}_o

| x Run | 0.524 | 0.873 | 1.57 | 1.82 | 2.32 | 2.82 | 3.32 | $\dot{q}(o)$ |
|------------|-------|-------|--------|--------|--------|--------|--------|--------------|
| 723 | 0.786 | 0.486 | 0.0767 | 0.0584 | 0.0488 | 0.0413 | | 34.4 |
| 724 | 0.796 | 0.494 | 0.0734 | 0.0564 | 0.0468 | 0.0398 | | 41.7 |
| 725 | 0.791 | 0.484 | 0.0736 | 0.0531 | 0.0464 | 0.0383 | 0.0358 | 38.6 |
| 726 | 0.759 | 0.503 | 0.0744 | 0.0571 | 0.0470 | 0.0406 | 0.0345 | 29.5 |
| 727 | 0.791 | 0.484 | 0.0798 | 0.0609 | 0.0510 | 0.0421 | 0.0376 | 39.4 |
| 728 | 0.787 | 0.485 | 0.0773 | 0.0579 | 0.0501 | 0.0397 | 0.0373 | 37.5 |
| 729 | 0.771 | 0.495 | 0.0782 | 0.0556 | 0.0478 | 0.0370 | 0.0362 | 34.9 |

TABLE III
TUNNEL H EXPERIMENTAL DATA

a. 4-in.-diam Model Pressure Data, P/P_0'

| x Run | 0.262 | 0.524 | 0.889 | 1.22 | 1.57 | 1.82 | 2.32 | 2.82 | 3.32 | P_0' |
|----------|-------|-------|-------|-------|--------|--------|--------|--------|--------|--------|
| 1456 | 0.965 | 0.762 | 0.386 | 0.155 | 0.0437 | 0.0389 | 0.0328 | 0.0269 | 0.0243 | 0.695 |
| 1457 | 0.890 | 0.716 | 0.390 | 0.162 | 0.0492 | 0.0398 | 0.0334 | 0.0254 | 0.0227 | 0.284 |
| 1458 | 0.935 | 0.720 | 0.398 | 0.162 | 0.0484 | 0.0398 | 0.0330 | 0.0249 | 0.0239 | 0.349 |
| 1459 | 0.928 | 0.693 | 0.366 | 0.140 | 0.0416 | 0.0341 | 0.0309 | 0.0247 | 0.0229 | 0.756 |
| 1460 | 0.926 | 0.715 | 0.378 | 0.150 | 0.0428 | 0.0368 | 0.0328 | 0.0260 | 0.0237 | 0.787 |
| 1461 | 0.962 | 0.689 | 0.400 | 0.155 | 0.0492 | 0.0378 | 0.0324 | 0.0241 | 0.0223 | 0.330 |
| 1462 | 0.962 | 0.700 | 0.398 | 0.151 | 0.0445 | 0.0350 | 0.0324 | 0.0249 | 0.0231 | 0.744 |
| 1463 | 0.985 | 0.785 | 0.431 | 0.156 | 0.0461 | 0.0379 | 0.0329 | 0.0256 | 0.0248 | 0.775 |
| 1464 | 0.980 | 0.734 | 0.406 | 0.157 | 0.0437 | 0.0357 | 0.0327 | 0.0254 | 0.0238 | 0.708 |
| 1465 | 0.980 | 0.680 | 0.392 | 0.147 | 0.0427 | 0.0348 | 0.0294 | 0.0245 | 0.0226 | 0.734 |

b. 1-in.-diam Model Pressure Data, P/P_0'

| x Run | 2.17 | P_0' |
|----------|--------|--------|
| 1431 | 0.0385 | 0.634 |
| 1432 | 0.0384 | 0.607 |

UNCLASSIFIED

Security Classification

DOCUMENT CONTROL DATA - R&D

(Security classification of title, body of abstract and indexing annotation must be entered when the overall report is classified)

| | |
|---|--|
| 1. ORIGINATING ACTIVITY (Corporate author) Arnold Engineering Development Center (AEDC) ARO, Inc. Operating Contractor Arnold Air Force Station, Tennessee | 2a. REPORT SECURITY CLASSIFICATION UNCLASSIFIED 2b. GROUP N/A |
|---|--|

3. REPORT TITLE
COMBINED EFFECTS OF VISCOUS INTERACTION AND IDEAL SOURCE FLOW ON PRESSURE AND HEAT-TRANSFER DISTRIBUTIONS OVER HEMISPHERE CYLINDERS AT $M_{\infty} \sim 18$

4. DESCRIPTIVE NOTES (Type of report and inclusive dates)
 N/A

5. AUTHOR(S) (Last name, first name, initial)
 Eaves, R. H., Jr. and Lewis, Clark H.

This document has been approved for public release its distribution is unlimited Per DDC ITR-75/5 AD A011700 Dtd July 1975

| | | |
|-----------------------------|------------------------------|-----------------------|
| 6. REPORT DATE July 1965 | 7a. TOTAL NO. OF PAGES 32 | 7b. NO. OF REFS 14 |
|-----------------------------|------------------------------|-----------------------|

| | |
|---|---|
| 8a. CONTRACT OR GRANT NO. AF40(600)-1200 b. PROJECT NO. 8953 c. Program Element 62405334 d. Task 895303 | 9a. ORIGINATOR'S REPORT NUMBER(S) AEDC-TR-65-158 9b. OTHER REPORT NO(S) (Any other numbers that may be assigned this report) N/A |
|---|---|

10. AVAILABILITY/LIMITATION NOTICES
~~Qualified requesters may obtain copies of this report from DDC.~~

| | |
|--------------------------------|--|
| 11. SUPPLEMENTARY NOTES N/A | 12. SPONSORING MILITARY ACTIVITY Arnold Engineering Development Center (AEDC), Air Force Systems Command (AFSC), Arnold Air Force Station, Tennessee |
|--------------------------------|--|

13. ABSTRACT

The combined effects of ideal source flow and viscous interaction on the pressure and heat-transfer distributions over hemisphere-cylinders are presented, and a comparison is made with experimental data from two of the AEDC-VKF hotshot tunnels. Ideal gas characteristics solutions for the inviscid flow field over the hemisphere-cylinders were obtained for ideal source flow fields matched to the tunnel geometry. The inviscid and viscous (laminar boundary layer) flow fields were iterated, and the resulting pressure and heat-transfer distributions were compared with the experimental data. Ideal gas analyses made at $M_{\infty} = 18$ predicted pressure and heat-transfer distributions over a 4-in.-diam model in the 100-in. hotshot Tunnel F, and pressure distributions for a similar model in the 50-in. hotshot Tunnel H were found in reasonably good agreement with the experimental data.

| | | | | | | | |
|-----|-----------|--------|----|--------|----|--------|----|
| 14. | KEY WORDS | LINK A | | LINK B | | LINK C | |
| | | ROLE | WT | ROLE | WT | ROLE | WT |
| | | | | | | | |

cylinders
pressure
heat transfer
wind tunnels
hypersonic flow

INSTRUCTIONS

1. ORIGINATING ACTIVITY: Enter the name and address of the contractor, subcontractor, grantee, Department of Defense activity or other organization (*corporate author*) issuing the report.

2a. REPORT SECURITY CLASSIFICATION: Enter the overall security classification of the report. Indicate whether "Restricted Data" is included. Marking is to be in accordance with appropriate security regulations.

2b. GROUP: Automatic downgrading is specified in DoD Directive 5200.10 and Armed Forces Industrial Manual. Enter the group number. Also, when applicable, show that optional markings have been used for Group 3 and Group 4 as authorized.

3. REPORT TITLE: Enter the complete report title in all capital letters. Titles in all cases should be unclassified. If a meaningful title cannot be selected without classification, show title classification in all capitals in parentheses immediately following the title.

4. DESCRIPTIVE NOTES: If appropriate, enter the type of report, e.g., interim, progress, summary, annual, or final. Give the inclusive dates when a specific reporting period is covered.

5. AUTHOR(S): Enter the name(s) of author(s) as shown on or in the report. Enter last name, first name, middle initial. If military, show rank and branch of service. The name of the principal author is an absolute minimum requirement.

6. REPORT DATE: Enter the date of the report as day, month, year; or month, year. If more than one date appears on the report, use date of publication.

7a. TOTAL NUMBER OF PAGES: The total page count should follow normal pagination procedures, i.e., enter the number of pages containing information.

7b. NUMBER OF REFERENCES: Enter the total number of references cited in the report.

8a. CONTRACT OR GRANT NUMBER: If appropriate, enter the applicable number of the contract or grant under which the report was written.

8b, 8c, & 8d. PROJECT NUMBER: Enter the appropriate military department identification, such as project number, subproject number, system numbers, task number, etc.

9a. ORIGINATOR'S REPORT NUMBER(S): Enter the official report number by which the document will be identified and controlled by the originating activity. This number must be unique to this report.

9b. OTHER REPORT NUMBER(S): If the report has been assigned any other report numbers (*either by the originator or by the sponsor*), also enter this number(s).

10. AVAILABILITY/LIMITATION NOTICES: Enter any limitations on further dissemination of the report, other than those

imposed by security classification, using standard statements such as:

- (1) "Qualified requesters may obtain copies of this report from DDC."
- (2) "Foreign announcement and dissemination of this report by DDC is not authorized."
- (3) "U. S. Government agencies may obtain copies of this report directly from DDC. Other qualified DDC users shall request through _____."
- (4) "U. S. military agencies may obtain copies of this report directly from DDC. Other qualified users shall request through _____."
- (5) "All distribution of this report is controlled. Qualified DDC users shall request through _____."

If the report has been furnished to the Office of Technical Services, Department of Commerce, for sale to the public, indicate this fact and enter the price, if known.

11. SUPPLEMENTARY NOTES: Use for additional explanatory notes.

12. SPONSORING MILITARY ACTIVITY: Enter the name of the departmental project office or laboratory sponsoring (*paying for*) the research and development. Include address.

13. ABSTRACT: Enter an abstract giving a brief and factual summary of the document indicative of the report, even though it may also appear elsewhere in the body of the technical report. If additional space is required, a continuation sheet shall be attached.

It is highly desirable that the abstract of classified reports be unclassified. Each paragraph of the abstract shall end with an indication of the military security classification of the information in the paragraph, represented as (TS), (S), (C), or (U).

There is no limitation on the length of the abstract. However, the suggested length is from 150 to 225 words.

14. KEY WORDS: Key words are technically meaningful terms or short phrases that characterize a report and may be used as index entries for cataloging the report. Key words must be selected so that no security classification is required. Identifiers, such as equipment model designation, trade name, military project code name, geographic location, may be used as key words but will be followed by an indication of technical context. The assignment of links, rules, and weights is optional.